Robust Coherent Transport of Light in Multilevel Hot Atomic Vapors

N. Cherroret,[1] M. Hemmerling,[2,3] V. Nador,[3] J. T. M. Walraven,[4] and R. Kaiser[3]
[1]*Laboratoire Kastler Brossel, Sorbonne Université, CNRS, ENS-PSL University, Collège de France, 4 Place Jussieu, 75005 Paris, France*
[2]*Instituto de Física de São Carlos, Universidade de São Paulo, 13560-970 São Carlos, São Paulo, Brazil*
[3]*Université Côte d'Azur, CNRS, Institut de Physique de Nice, Valbonne F-06560, France*
[4]*Van der Waals-Zeeman Institute, Institute of Physics, University of Amsterdam, Science Park 904, 1098 XH Amsterdam, The Netherlands*

(Received 21 December 2018; published 7 May 2019)

Using a model system, we demonstrate both experimentally and theoretically that coherent scattering of light can be robust in hot atomic vapors despite a significant Doppler effect. By operating in a linear regime of far-detuned light scattering, we also unveil the emergence of interference triggered by inelastic Stokes and anti-Stokes transitions involving the atomic hyperfine structure.

DOI: 10.1103/PhysRevLett.122.183203

Coherent transport in disordered media is at the focus of intense investigations in many fields of research, including condensed matter [1], astrophysics [2], acoustics [3], optics [4], atomic physics [5], and ultracold atoms [6]. In these fields, many coherence-related phenomena are often not fully controlled and described by effective parameters. In particular, treatments of light propagation in atomic vapors often leave aside the internal atomic structure and use a simplified two-level model. Interestingly, in cases when the detailed structure is accounted for, not only the quantitative description is improved, but new qualitative features emerge, such as Sisyphus cooling [7], slow light [8], and quantum memories [9]. Another ingredient adding to the complexity of light propagation in these systems is Doppler broadening. With the impressive improvement of high-precision measurements allowed by the development of atom laser cooling, a fine, microscopic description of temperature effects has become crucial. A well-known example is collective phenomena in nearby coupled dipoles [10–15], which involve Doppler-sensitive interference. This question is also central in room temperature atomic vapors, which have seen a renewed interest in precision measurements, including applications on electric-field sensors [16] and quantum information [17–20]. In hot vapors, it is commonly thought that interference is washed out by Doppler broadening and a radiative transfer equation is often used as a simplified model [5]. This description, however, misses many intriguing phenomena like collective lamb shifts [15] or the polarization anomaly at the $D1$ line of the solar spectrum [21]. In this Letter, we show that thermal decoherence in hot atomic vapors can be largely circumvented by operating in the large detuning limit, where atomic motion is negligible during scattering events. In this regime, we also discover that the multilevel atomic structure leads to a new interference mechanism based on inelastic Raman scattering from hyperfine levels, which we describe with a quantitatively accurate microscopic theory.

Our experiment is sketched in Fig. 1. A collimated laser beam (waist $w = 10$ mm) is sent through a slab-shaped glass cell containing a natural mixture of rubidium vapor at an oven-regulated temperature and density. The wavelength $\lambda = 780$ nm is set to the $D2$ transition of rubidium. Two cells were used, one with a metallic mirror clipped to the back side and another one without such a mirror. The angle of incidence of the laser beam $\theta_0 \ll 1$ was adjusted to typically a few tens of milliradians with respect to the surface normal of the slab. The backscattered light was observed in the far field with an optical angular resolution of 0.044 mrad using a charge-coupled device (CCD)

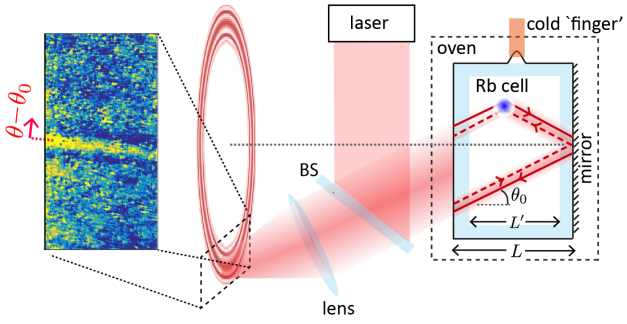

FIG. 1. Experimental scheme (for clarity, polarization elements are not shown). A collimated laser beam is sent via a beam splitter (BS) through a glass cell (width $L \simeq 8$ mm, chamber thickness $L' \simeq 6$ mm) containing a hot rubidium mixture. An oven with a cold "finger" is used to regulate the vapor pressure in the cell. The backscattered signal is collected in the far field on a CCD camera. In the cell, the interference between counterpropagating wave paths scattered on both an atom and the back face of the cell gives rise to annular fringes ("mirror-assisted coherent backscattering").

camera (Fig. 1). Because of light scattering, this signal has generically two types of contributions: the "incoherent" ones, associated with in-phase pairs of paths traveling along an identical sequence of scatterers, and the "coherent" ones, where the two paths accumulate a finite phase difference [22]. In the multiple scattering regime, the latter leads, in particular, to the coherent backscattering effect, which was previously measured in cold atomic gases [23]. Our goal is to investigate the coherent component of the signal in a hot vapor. For this purpose, the cell is heated to temperatures on the order of 200 °C. In this regime, the atomic motion is very fast, which *a priori* constitutes an unfavorable case for coherent transport. Indeed, the Doppler effect associated with thermal motion induces a random frequency shift in scattered wave paths, a phase-breaking mechanism usually detrimental to interference [24,25]. To counteract this mechanism, our strategy has been to operate at large detuning $|\Delta \equiv \omega - \omega_0| \gg k\bar{v}$ so that the characteristic time $\sim\lambda/\bar{v}$ for an atom to move over a wavelength becomes much longer than the time $\tau \sim \Gamma^{-1}(\Gamma/\Delta)^2$ of a scattering process (ω and ω_0 are the laser and atomic angular frequencies, Γ is the natural linewidth, $k = 2\pi/\lambda$ is the wave number, and $\bar{v} = \sqrt{k_B T/m}$ is a measure for the atomic thermal speed). The left panel of Fig. 1 shows a typical experimental CCD image, obtained at $T \simeq 195\,°\mathrm{C}$ and $|\Delta| = 2$ GHz [26,27]. Under these conditions, $|\Delta|/k\bar{v} \simeq 7.3 \gg 1$ and $k\bar{v}/\Gamma \simeq 45 \gg 1$. Despite the large Doppler effect, the image in Fig. 1 displays a well contrasted interference fringe, suggesting that atoms effectively behave like cold ones. This fringe stems from the interference between counterpropagating wave paths scattered on both an atom and the mirror on the back face of the cell, as illustrated in Fig. 1. It leads to an interference ring known as the mirror-assisted coherent backscattering (m-CBS) effect [28–30], on which we will concentrate our attention from now on. While m-CBS was recently measured in a cold strontium gas [30], its visibility in a *hot* rubidium vapor with highly nontrivial quantum-level structure is far from obvious. To understand it, we have analytically calculated the enhancement factor $\Lambda \equiv (S_b + S_{\text{m-CBS}})/S_b$ of the m-CBS signal $S_{\text{m-CBS}}$ with respect to the incoherent background signal S_b, taking into account the thermal distribution of atomic velocities (see the Supplemental Material [31])

$$\Lambda(\theta, T) = 1 + \Lambda_0 \exp\left[-2\left(\frac{k\bar{v}\theta_0 L}{\Gamma\ell}\right)^2\right] \times \cos[kL(\theta-\theta_0)\theta_0]\mathrm{sinc}[kL'(\theta-\theta_0)\theta_0], \quad (1)$$

where $\theta - \theta_0$ is the angular deviation from the fringe maximum (see Fig. 1) and $\Lambda_0 \equiv \Lambda(\theta_0, T = 0) - 1$. Equation (1) indeed describes an interference ring, with radial oscillations governed by two length scales, the distance $L/2$ from the center of the cell to the mirror, and the thickness L' of the vapor [30]. The exponential factor stems from the thermal average of the dephasing $e^{i\Delta\Phi_T}$ accumulated by the two interfering paths, whose frequency is Doppler shifted by $\boldsymbol{v}\cdot\Delta\boldsymbol{k}$ upon scattering with momentum change $\Delta\boldsymbol{k}$ on an atom of velocity $\boldsymbol{v}$,

$$\Delta\Phi_T \sim L\boldsymbol{v}\cdot\Delta\boldsymbol{k}\frac{\partial k}{\partial\omega} \sim \frac{Lk\bar{v}\theta_0}{\Gamma\ell}, \quad (2)$$

where we used that $\partial k/\partial\omega \sim 1/\Gamma\ell$ when $|\Delta| \gg \Gamma$, with ℓ as the mean free path. Equation (2) explains the robustness of the m-CBS interference against thermal motion. First, since $|\Delta| \gg k\bar{v}$, we have $\ell \simeq \ell(\bar{v} = 0) \propto k^2\rho^{-1}(\Delta/\Gamma)^2$, where ρ is the atom density. The impact of dephasing is thus lessened at large detuning. The second reason lies in the proportionality of $\Delta\Phi_T$ to the incident angle $\theta_0 \ll 1$: as we operate near normal incidence, scattering is essentially forward ($\Delta\boldsymbol{k} \sim 0$), which again reduces $\Delta\Phi_T$. Figure 2 shows a typical experimental angular profile $\Lambda(\theta, T)$ of the m-CBS ring (blue dots). To obtain these data, we have measured both the background S_b and m-CBS $S_{\text{m-CBS}}$ signals, from which we have removed stray light by subtracting the signal at $|\Delta| = 40$ GHz. The profile is compared with Eq. (1), shown as a solid red curve. For this comparison, the amplitude at $\theta = \theta_0$, $\Lambda(\theta_0, T)$, is set to the experimental value 1.20. Except for this reference point though, there is no adjustable parameter: the agreement for the width of the central fringe and even for the first secondary fringes is excellent.

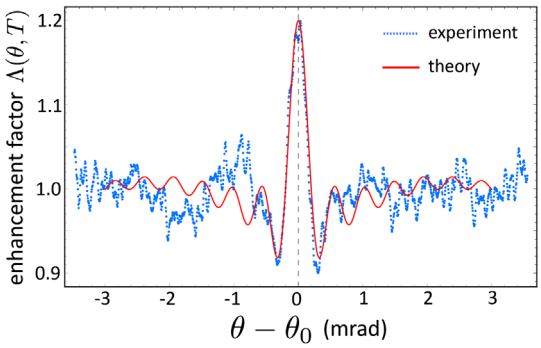

FIG. 2. Angular radial cut of the m-CBS interference ring (detuning $|\Delta| = 2$ GHz, incident angle $\theta_0 \simeq 7°$, polarization channel $h\perp h$). Blue dots are the experimental signal. The red curve is Eq. (1), in which the amplitude at $\theta = \theta_0$, $\Lambda(\theta_0, T)$, is set to the experimental value 1.20. Except for this reference point, there is no adjustable parameter.

The most interesting property of Eq. (2) is the dependence of $\Delta\Phi_T$ on the mean free path $\ell \propto (\Delta/\Gamma)^2$. This offers the possibility to turn from a hot to a cold atom behavior in a controlled way via a change of the detuning. To check this property, we have measured the m-CBS enhancement factor $\Lambda(\theta = \theta_0, T)$ as a function of $|\Delta|$ over a broad range. The results are presented in Fig. 3. The curves correspond to three detection schemes, where linearly polarized light is analyzed along the parallel ($l\|l$) or

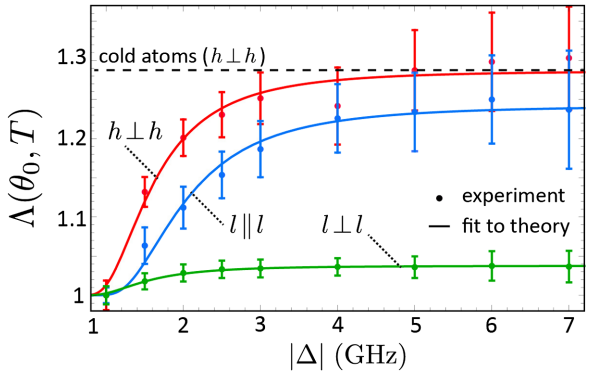

FIG. 3. m-CBS enhancement factor $\Lambda(\theta_0, T)$ as a function of detuning in three polarization channels. The experimental data (dots) are fitted with Eq. (1) at $\theta = \theta_0$, using Λ_0 and ρk^{-3} as fit parameters (solid curves). These fits provide $\rho k^{-3} = 0.15$, 0.22, 0.14 and $\Lambda_0 = 0.038$, 0.242, and 0.287 in the channels $l\perp l$, $l\parallel l$, and $h\perp h$, respectively. No signal is observed in the channel $h\parallel h$. The dashed line shows the enhancement factor expected for cold atoms (i.e., in the limit $k\bar{v}/\Gamma \to 0$) in the channel $h\perp h$.

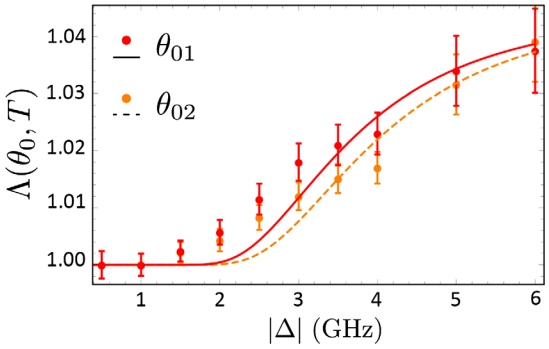

FIG. 4. m-CBS enhancement factor $\Lambda(\theta_0, T)$ vs detuning at two incident angles $\theta_0 = \theta_{01}$ and $\theta_{02} > \theta_{01}$, in the channel $h\perp h$ at fixed $T \simeq 168°$. Dots are experimental points and curves are fits to Eq. (1).

perpendicular ($l\perp l$) channels, or where circularly polarized light is analyzed in the channel of opposite ($h\perp h$) helicity [23,32], as routinely done in experiments on light scattering in random media. No signal is observed in the channel $h\parallel h$ because, at large detuning, the excited hyperfine levels of the $D2$ line of rubidium are not resolved, so that the single scattering process is essentially equivalent to a $J = 1/2 \to 3/2$ transition [33]. Let us first discuss the variation of the curves with detuning. We attribute it to the exponential factor in Eq. (1). Fits of the experimental data to Eq. (1) (solid curves in Fig. 3) validate this interpretation and demonstrate our ability to control the thermal dephasing via the detuning in the vapor. For comparison, in the channel $h\perp h$ we also show as a dashed line the enhancement $\Lambda(\theta_0, T = 0) = 1 + \Lambda_0$ expected for cold atoms. In fact, Fig. 3 indicates that the "cold atom limit" is almost reached for $\Delta \gtrsim 4$ GHz whatever the polarization configuration.

For the fits to Eq. (1), we use Λ_0 and ρk^{-3} as free parameters and extract a nearly constant parameter $\rho k^{-3} = 0.17 \pm 0.05$, which confirms the independence of the dephasing (2) upon polarization. The relative values of enhancement factors in the various polarization channels thus stem from the zero-temperature amplitude $\Lambda_0 = S_{\text{m-CBS}}/S_b$. We attribute them to the proportionality of the m-CBS signal $S_{\text{m-CBS}}(T = 0)$ to the elastic differential cross section $d\sigma_{\text{el}}/d\Omega$, assuming that the background signal $S_b(T = 0)$ is independent of polarization. Except at low detuning, this assumption is approximately verified in our setup. For an incident wave whose polarization vector changes from $\boldsymbol{\epsilon}_{\text{in}}$ to $\boldsymbol{\epsilon}_{\text{out}}$ upon scattering on an atom, it was shown, based on the decomposition of the scattered intensity into irreducible components with respect to the rotation group, that $d\sigma_{\text{el}}/d\Omega \propto w_1|\boldsymbol{\epsilon}_{\text{in}} \cdot \boldsymbol{\epsilon}^*_{\text{out}}|^2 + w_2|\boldsymbol{\epsilon}_{\text{in}} \cdot \boldsymbol{\epsilon}_{\text{out}}|^2 + w_3$ [34,35]. The numerical coefficients w_i depend on the fine and hyperfine level structure of rubidium. We have calculated them using the approach developed in [33] for treating light scattering from hyperfine multiplets. From this calculation, we evaluate the ratios $\Lambda_0(h\perp h)/\Lambda_0(l\parallel l) \simeq 1.1$ and $\Lambda_0(l\parallel l)/\Lambda_0(l\perp l) \simeq 8.0$ [36], in reasonable agreement with the experimental ratios extracted from the fits in Fig. 3: $\Lambda_0^{\text{exp}}(h\perp h)/\Lambda_0^{\text{exp}}(l\parallel l) \simeq 1.2$ and $\Lambda_0^{\text{exp}}(l\parallel l)/\Lambda_0^{\text{exp}}(l\perp l) \simeq 6.4$.

According to Eq. (1), the thermal dephasing (2) can be also controlled with the incident angle θ_0. To verify this property, we have measured the m-CBS enhancement factor as a function of detuning for two different angles $\theta_{01} \simeq 6.5°$ and $\theta_{02} \simeq 7.5° > \theta_{01}$ deduced from the m-CBS angular profiles. These measurements are displayed in Fig. 4 (dots). We fit them with Eq. (1) with Λ_0 as a single fit parameter (solid and dashed curves), inferring the atom density ρ from the saturated vapor pressure in the cell. For these measurements, we used another atomic cell heated to $T \simeq 168$°C and on which no mirror was clipped on the back face (the glass itself thus plays the role of the mirror). Λ_0 being also proportional to the reflection coefficient of the glass [30], much smaller than the one of the mirror, this leads to smaller enhancement factors than in Fig. 3.

In the description of the m-CBS interference presented so far, we implicitly assumed that light was scattered *elastically* on the atom (Rayleigh scattering). As we operate at a large detuning $|\Delta| \gg \Gamma$ though, the light-matter interaction may involve atomic transitions where several hyperfine levels come into play, such that it is not guaranteed that only Rayleigh scattering occurs. A quick look at the typical level structure of rubidium, recalled in Fig. 5(b), confirms this statement: the structure involves two ground-state levels F and $F + 1$, the various Zeeman sublevels of which are equally populated in our hot vapor. When subjected to light, atoms may experience Rayleigh transitions $F \to F$ or $F + 1 \to F + 1$ via any of the allowed excited levels [the Rayleigh transition $F + 1 \to F + 1$ is illustrated in Fig. 5(b)]. These processes, whose strength is encapsulated in the elastic scattering cross

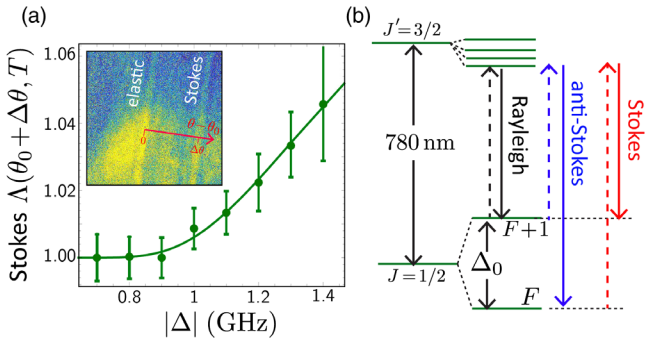

FIG. 5. (Inset) CCD image showing a secondary m-CBS ring associated with inelastic scattering, here visible in the channel $l\perp l$ at $|\Delta| = 1.3$ GHz. The red arrow is the $\theta - \theta_0$ axis; the secondary ring is maximum at $\theta = \Delta\theta + \theta_0$. (a) Experimental enhancement factor $\Lambda(\theta = \theta_0 + \Delta\theta, T)$ of the secondary ring vs detuning (dots), together with a fit to Eq. (3). (b) Level structure of rubidium. In addition to elastic (Rayleigh) processes, at large detuning light can experience inelastic (Stokes and anti-Stokes) processes from the two ground-state levels separated by Δ_0 [$\Delta_0 = 3.0$ GHz (6.8 GHz) and $F = 2$ ($F = 1$) for ^{85}Rb (^{87}Rb)].

section, yield the elastic m-CBS ring discussed previously. Since Δ is large compared to the typical spacing between the excited hyperfine levels, those are not resolved in our experiment. Δ is, on the other hand, *not* small compared to the spacing Δ_0 between the two ground-state levels F and $F+1$. This implies that Stokes ($F \to F+1$) and anti-Stokes ($F+1 \to F$) *inelastic* scattering processes can occur as well [see Fig. 5(b)]. Note that this type of inelastic transition here shows up in the *linear* regime of light scattering (small saturation parameter) and is thus fundamentally different from the inelastic processes that occur at higher intensities [37–40]. A refined analytical calculation of the m-CBS effect (see the Supplemental Material [31]) shows that these Stokes–anti-Stokes transitions give rise to two *secondary* interference rings, of enhancement factor

$$\Lambda(\theta,T) = 1 + \Lambda_0 \exp\left[-2\left(\frac{k\bar{v}\theta_0 L}{\Gamma\ell}\right)^2\right] \times \cos[kL(\theta-\theta_0)\theta_0 + L\Delta k] \times \mathrm{sinc}[kL'(\theta-\theta_0)\theta_0 + L\Delta k]. \quad (3)$$

As compared to Eq. (1), an additional momentum shift Δk arises because the light frequency changes by $\pm\Delta_0$ after Stokes or anti-Stokes scattering on the atom. This shift is given by

$$\Delta k = k[n(\Delta \pm \Delta_0) - n(\Delta)], \quad (4)$$

with a plus (minus) sign for the anti-Stokes (Stokes) process. In Eq. (4), n is the refractive index of the gas. The momentum shift in Eq. (3) implies that inelastic rings are angularly separated by $\Delta\theta \simeq -\Delta k/(k\theta_0)$ from the elastic one. They are visible in polarization channels where inelastic scattering is present. We have found from calculations of inelastic scattering cross sections that this is typically the case in the channel $l\perp l$, where we have experimentally focused our attention. In the inset of Fig. 5(a), we show a CCD image taken at $\Delta = -1.3$ GHz and $T \simeq 166$°C in this channel: we indeed observe a secondary fringe close to the elastic one. To demonstrate that it is well of m-CBS type, we have tested its sensitivity to thermal dephasing. The plot in Fig. 5(a) confirms this sensitivity: the enhancement factor $\Lambda(\theta_0 + \Delta\theta, T)$ of the inelastic fringe vs Δ is well fitted by Eq. (3). From this fit we extract $\rho k^{-3} \simeq 0.16$, which we use to estimate the ring separation $\Delta\theta$. Assuming a Stokes process (a choice justified below) and estimating the refractive index for a dilute atomic cloud (see the Supplemental Material [31]), we find $\Delta\theta = 0.28°$ from Eq. (4) [41]. This value is on the order of the experimental one, $\Delta\theta_{\mathrm{exp}} = 0.15°$, measured on the camera image. A possible reason for the theoretical overestimation is the uncertainty on ρk^{-3}. One may wonder, finally, why only one inelastic fringe is visible in the inset of Fig. 5, while Eq. (4) in principle predicts two fringes. The reason lies in the frequency asymmetry of the Stokes and anti-Stokes transitions. Indeed, unlike the Stokes process, the anti-Stokes process brings photons back to resonance [27]. This leads to a large momentum shift (4), which moves the anti-Stokes ring far away from the elastic one, out of the range of the camera [from Eq. (4) we estimate $\Delta\theta_{\text{anti-Stokes}} \sim -10\Delta\theta_{\text{Stokes}}$). Note that the Stokes nature of the secondary fringe in Fig 5(a) is also confirmed by its position with respect to the elastic one: for the Stokes process $n(\Delta - \Delta_0) - n(\Delta) < 0$ so that $\Delta\theta > 0$.

By operating at large detuning, we have shown that elementary interference between optical paths can survive in hot atomic vapors. This finding could be exploited to enhance more complex interference phenomena under conditions of large Doppler effect, as well as collective interference effects like subradiance, so far only observed in cold gases [10]. We have also unveiled a novel interference mechanism based on inelastic scattering from hyperfine levels in the linear regime. This sheds light on the important role Raman processes might play in multiple scattering [42], a question yet largely unexplored in ensembles of quantum scatterers.

N. C. thanks Dominique Delande for helpful discussions. We also acknowledge financial support from the Agence Nationale de la Recherche (Grant No. ANR-14-CE26-0032 LOVE). This work was conducted within the framework of the project OPTIMAL granted by the European Union by means of the Fond européen de développement régional, FEDER.

[1] E. Akkermans and G. Montambaux, *Mesoscopic Physics of Electrons and Photons* (Cambridge University Press, Cambridge, England, 2007).

[2] H. C. Van de Hulst, *Multiple Light Scattering: Tables, Formulas, and Applications* (Elsevier, New York, 2012).
[3] H. Hu, A. Strybulevych, J. Page, S. Skipetrov, and B. van Tiggelen, Nat. Phys. **4**, 945 (2008).
[4] S. Rotter and S. Gigan, Rev. Mod. Phys. **89**, 015005 (2017).
[5] A. F. Molisch and B. P. Oehry, *Radiation Trapping in Atomic Vapors* (Clarendon Press, Oxford, 1998).
[6] A. Aspect and M. Inguscio, Phys. Today **62**, No. 8, 30 (2009).
[7] J. Dalibard and C. Cohen-Tannoudji, J. Opt. Soc. Am. B **11**, 2043 (1989).
[8] L. V. Hau, S. E. Harris, Z. Dutton, and C. H. Behroozi, Nature (London) **397**, 594 (1999).
[9] L. M. Duan, M. D. Lukin, J. I. Cirac, and P. Zoller, Nature (London) **414**, 413 (2001).
[10] W. Guérin, M. O. Araùjo, and R. Kaiser, Phys. Rev. Lett. **116**, 083601 (2016).
[11] J. Pellegrino, R. Bourgain, S. Jennewein, Y. R. P. Sortais, A. Browaeys, S. D. Jenkins, and J. Ruostekoski, Phys. Rev. Lett. **113**, 133602 (2014).
[12] S. Jennewein, M. Besbes, N. J. Schilder, S. D. Jenkins, C. Sauvan, J. Ruostekoski, J.-J. Greffet, Y. R. P. Sortais, and A. Browaeys, Phys. Rev. Lett. **116**, 233601 (2016).
[13] L. Corman, J. L. Ville, R. Saint-Jalm, M. Aidelsburger, T. Bienaimé, S. Nascimbène, J. Dalibard, and J. Beugnon, Phys. Rev. A **96**, 053629 (2017).
[14] R. Saint-Jalm, M. Aidelsburger, J. L. Ville, L. Corman, Z. Hadzibabic, D. Delande, S. Nascimbène, N. Cherroret, J. Dalibard, and J. Beugnon, Phys. Rev. A **97**, 061801(R) (2018).
[15] T. Peyrot, Y. R. P. Sortais, A. Browaeys, A. Sargsyan, D. Sarkisyan, J. Keaveney, I. G. Hughes, and C. S. Adams, Phys. Rev. Lett. **120**, 243401 (2018).
[16] J. A. Sedlacek, A. Schwettmann, H. Kübler, and J. P. Shaffer, Phys. Rev. Lett. **111**, 063001 (2013).
[17] A. Urvoy, F. Ripka, I. Lesanovsky, D. Booth, J. P. Shaffer, T. Pfau, and R. Löw, Phys. Rev. Lett. **114**, 203002 (2015).
[18] D. J. Whiting, N. Sibalic, J. Keaveney, C. S. Adams, and I. G. Hughes, Phys. Rev. Lett. **118**, 253601 (2017).
[19] C. B. Moller, R. A. Thomas, G. Vasilakis, E. Zeuthen, Y. Tsaturyan, M. Balabas, K. Jensen, A. Schliesser, K. Hammerer, and E. S. Polzik, Nature (London) **547**, 191 (2017).
[20] R. Jiménez-Martínez, J. Kolodynski, C. Troullinou, V. G. Lucivero, J. Kong, and M. W. Mitchell, Phys. Rev. Lett. **120**, 040503 (2018).
[21] J. O. Stenflo, Astrophys. J. **801**, 70 (2015).
[22] P. Sheng, *Introduction to Wave Scattering, Localization, and Mesoscopic Phenomena* (Academic Press, New York, 1995).
[23] G. Labeyrie, F. de Tomasi, J.-C. Bernard, C. A. Müller, Ch. Miniatura, and R. Kaiser, Phys. Rev. Lett. **83**, 5266 (1999).
[24] A. A. Golubentsev, Sov. Phys. JETP **59**, 26 (1984).
[25] G. Labeyrie, D. Delande, R. Kaiser, and C. Miniatura, Phys. Rev. Lett. **97**, 013004 (2006).
[26] Here and in the rest of the Letter, temperatures are given with an uncertainty of about 10 °C.
[27] For convenience, in the experiment we choose to work with negative detunings.
[28] J.-J. Greffet, Waves Random Media **1**, S65 (1991).
[29] G. Labeyrie, C. A. Müller, D. S. Wiersma, C. Miniatura, and R Kaiser, J. Opt. B **2**, 672 (2000).
[30] P. H. Moriya, R. F. Shiozaki, R. Celistrino Teixeira, C. E. Máximo, N. Piovella, R. Bachelard, R. Kaiser, and Ph. W. Courteille, Phys. Rev. A **94**, 053806 (2016).
[31] See Supplemental Material at http://link.aps.org/supplemental/10.1103/PhysRevLett.122.183203 for a derivation of Eqs. (1) and (3) and for the exact expression of the mean free path and refractive index used for the fits.
[32] P. E. Wolf, G. Maret, E. Akkermans, and R. Maynard, J. Phys. II (France) **49**, 63 (1988).
[33] C. A. Müller, C. Miniatura, D. Wilkowski, R. Kaiser, and D. Delande, Phys. Rev. A **72**, 053405 (2005).
[34] A. Omont, Prog. Quantum Electron. **5**, 69 (1977).
[35] C. A. Müller and C. Miniatura, J. Phys. A **35**, 10163 (2002).
[36] N. Cherroret *et al.* (to be published).
[37] B. R. Mollow, Phys. Rev. **188**, 1969 (1969).
[38] T. Wellens, B. Grémaud, D. Delande, and C. Miniatura, Phys. Rev. A **70**, 023817 (2004).
[39] V. Shatokhin, C. A. Müller, and A. Buchleitner, Phys. Rev. Lett. **94**, 043603 (2005).
[40] T. Binninger, V. N. Shatokhin, A. Buchleitner, and T. Wellens, arXiv:1811.08882.
[41] This value corresponds to the isotope ^{85}Rb for which $\Delta_0 = 3.0$ GHz. The isotope ^{87}Rb, for which $\Delta_0 = 6.8$ GHz, in principle, gives rise to an extra Stokes ring but with larger separation $\Delta\theta \simeq 0.37°$.
[42] B. Fazio, A. Irrera, S. Pirotta, C. D'Andrea, S. Del Sorbo, M. J. Lo Faro, P. G. Gucciardi, M. A. Iatì, R. Saija, M. Patrini, P. Musumeci, C. S. Vasi, D. S. Wiersma, M. Galli, and F. Priolo, Nat. Photonics **11**, 170 (2017).